Mon. Not. R. Astron. Soc. **267**, 209–224 (1994)

Helioseismic measurement of the extent of overshoot below the solar convection zone

Sarbani Basu, H. M. Antia and D. Narasimha
Tata Institute of Fundamental Research, Homi Bhabha Road, Bombay 400 005, India

Accepted 1993 October 7. Received 1993 October 5; in original form 1993 April 28

ABSTRACT

The discontinuity in the derivatives of the sound speed at the base of the overshoot layer below the solar convection zone introduces a characteristic oscillatory component in the frequencies of solar p-modes as a function of the radial order n. The amplitude of this oscillatory part is calibrated as a function of the extent of overshoot using a sequence of solar models constructed with varying extent of overshoot. Using this calibration, an attempt is made to measure the extent of overshoot below the solar convection zone using the available frequencies of the p-modes. It is found that the observed frequencies are consistent with a solar model without overshoot. Further, taking account of the errors in observations, it is possible to put a 2σ upper limit of $0.1\,H_p$ on the extent of overshoot.

Key words: convection – Sun: interior – Sun: oscillations.

1 INTRODUCTION

It is generally accepted that there is no adequate theory to describe astrophysical convection. In particular, there is no agreement among different theories about the extent of overshoot from stellar convection zones (Renzini 1987). From laboratory experiments and meteorological observations (cf. Townsend 1966; Deardorff, Willis & Lilly 1969) there is evidence for appreciable penetration of convective motions beyond the unstable region as determined by the Schwarzschild criterion. Similarly, numerical simulations of penetrative convection also show substantial overshoot (Hurlburt, Toomre & Massaguer 1986). The only overshoot layer in stars that is directly accessible to observations is the region above the solar photosphere, where again there is evidence for substantial overshoot (Keil & Canfield 1978). On the basis of these results, it is sometimes concluded that there is substantial overshoot below the solar convection zone, as well as beyond the convective cores of massive stars. Stothers & Chin (1992) have, however, analysed data involving the maximum effective temperature of hot evolved stars in certain clusters to conclude that the data are consistent with no overshoot from the convective cores in these stars. They also set an upper limit of $0.2\,H_p$ (where H_p is the local pressure scaleheight) for the extent of overshoot on the basis of their analysis. Similarly, using arguments based on the consistency of the mixing length theory, Antia & Chitre (1993) found an overshoot of about $0.1\,H_p$ below the solar convection zone. Clearly, since the overshoot layer below the solar convection zone is not directly observable, it would be interesting to estimate its thickness using the available helioseismic data (Libbrecht, Woodard & Kaufman 1990).

All reasonable models of convection dynamics (e.g. Zahn 1991) indicate that the overshoot layer below the base of the solar convection zone is almost adiabatically stratified and is followed by an almost discontinuous transition to radiative stratification below the base of the overshoot layer. Gough (1990) has shown that abrupt changes of this type contribute a characteristic oscillatory component to the frequencies $\nu_{n,\ell}$ of those p-modes that penetrate beyond the base of the overshoot layer. This oscillatory component can be extracted by taking second differences, $\delta^2\nu_{n,\ell}=\nu_{n+1,\ell}-2\nu_{n,\ell}+\nu_{n-1,\ell}$, of the frequencies with respect to the radial order n for a given degree ℓ. The amplitude of these oscillations depends on the 'severity' of the discontinuity, which in turn depends on the extent of overshoot. In models without any overshoot the first derivative of temperature ($\mathrm{d}T/\mathrm{d}r$), and hence that of the sound speed, is continuous, while the second derivative is discontinuous. This leads to a mild discontinuity at the base of the convection zone. On the other hand, in models with overshoot below the convection zone, the first derivative of the sound speed itself is discontinuous at the base of the

overshoot layer, where the temperature gradient jumps from the adiabatic to the radiative value. Further, the amount of discontinuity in the first derivative increases with the extent of overshoot. Thus the amplitude of these oscillations in the frequency can be calibrated as a function of the extent of overshoot by constructing solar models with different amounts of overshoot, and the extent of overshoot in the Sun may be surmised by comparing the amplitude obtained from solar oscillation data against the calibration.

Using this technique, Monteiro, Christensen-Dalsgaard & Thompson (1993a,b) tried to estimate the extent of overshoot below the solar convection zone. They found that the amplitude estimated using the observed frequencies is essentially consistent with a model without overshoot. The same conclusion was drawn by Gough & Sekii (1993) and Roxburgh & Vorontsov (1993). In fact, the amplitude from the solar data is slightly smaller than that for a solar model without overshoot, and hence it appears that the actual Sun may be even smoother than the model without overshoot. However, since the amplitude is fairly small, it is difficult to estimate the effect of errors in observed frequencies. Further, in addition to the oscillatory part, there is a smooth component of the frequency which is difficult to remove in an unambiguous manner. In fact, Berthomieu et al. (1993) considered the relative differences between observed solar frequencies and those computed for solar models to conclude that the solar data resemble more closely a model with overshoot than one without. Monteiro et al. (1993b) have pointed out that it may be difficult to draw any conclusions from a straightforward comparison of frequency differences between the Sun and a model, because of considerable uncertainties in the frequencies introduced by the outer layers of the solar convection zone, which are not very well understood. Clearly, it is necessary to perform an independent analysis of the data to ascertain the extent of overshoot below the solar convection zone. In particular, the systematic errors in the earlier studies can be estimated only by a study using an independent numerical procedure. Monteiro et al. (1993a) used the second difference of the frequency to extract the oscillatory part, while Monteiro et al. (1993b) extracted the oscillatory part directly from the frequencies. They do not, however, appear to have taken account of the fact that the amplitude of the oscillatory component can also be a function of ℓ. Roxburgh & Vorontsov (1993) attempted to measure the phase shift introduced at the base of the convection zone using a second-order asymptotic technique. They derived an upper limit of $0.35H_p$ on the extent of overshoot.

For the present work we have constructed a number of solar models with varying extent of overshoot and depth of the convection zone. For each of these models, the frequencies $\nu_{n,\ell}$ are computed and the amplitude of the oscillatory component is determined. Higher (fourth, sixth and eighth) order differences are used to extract the oscillatory component from the frequencies. The same exercise is repeated for the observed frequencies to find the amplitude of the oscillatory part, which can be compared against our models to determine the extent of overshoot in the Sun. Preliminary results from our work were presented in Basu, Antia & Narasimha (1993), where the variation of amplitude with ℓ was not accounted for. In the present work, we have included this variation, which results in significantly better fits.

2 THE BASIC TECHNIQUE

The basic principle behind this approach can be understood by considering a simple two-layer model (Gough 1990; Gough & Sekii 1993) with a discontinuity in both the sound speed and the Brunt–Väisälä frequency at the interface located at a radial distance of r_d. Let k_{r1} be the wavenumber in the region above $r=r_d$, where the wavefunction is of the form $B\sin(k_{r1}r)$. Similarly, let $k_{r2}^2=k_{r1}^2(1+\epsilon)$ be the wavenumber in the region below the discontinuity, where the wavefunction is of the form $C\sin(k_{r2}r+\phi)$. The local wavenumber k_r for solar oscillations is given by (Deubner & Gough 1984; Christensen-Dalsgaard & Berthomieu 1991)

$$k_r^2=\frac{\omega^2}{c^2}\left[1-\frac{\omega_c^2}{\omega^2}-\frac{S_\ell^2}{\omega^2}\left(1-\frac{N^2}{\omega^2}\right)\right], \tag{1}$$

where c is the sound speed and ω_c, N and S_ℓ are, respectively, the acoustic cut-off frequency, the Brunt–Väisälä frequency and the Lamb frequency. The phase shift ϕ introduced at $r=r_d$ can be estimated by demanding continuity of the wavefunction and its first derivative at $r=r_d$ to get

$$\tan(k_{r1}r_d)=\frac{\tan(k_{r1}r_d\sqrt{1+\epsilon}+\phi)}{\sqrt{1+\epsilon}}. \tag{2}$$

While deriving this expression we have neglected the term involving $\mathrm{d}H/\mathrm{d}r$ (where H is the scaleheight) in ω_c, which should behave like a delta function at the discontinuity, in models with overshoot. In the presence of this term, the derivative of the wavefunction will not be continuous, thus leading to some additional terms in equation (2) (Gough & Sekii 1993; Monteiro, Christensen-Dalsgaard & Thompson 1994). Apart from this, there could be other terms arising from the fact that the wavefunction is not strictly sinusoidal. For simplicity, we have neglected all these effects.

After some algebraic manipulation, it can be shown that, to the first order in ϵ, the phase shift can be written as

$$\phi\approx-\frac{1}{2}\epsilon k_{r1}r_d+\frac{\epsilon}{4}\sin(2k_{r1}r_d). \tag{3}$$

Application of the boundary condition at the lower boundary $r=r_0$ yields the dispersion relation

$$k_{r2}r_0+\phi=n\pi+\alpha, \tag{4}$$

where α is a suitable constant which is supposed to take care of the behaviour of the wavefunction near the turning points. This equation gives a relation between the oscillatory part in the frequency and that in the phase shift ϕ.

Although, in the simple model considered here, we assume a discontinuity in the sound speed at the base of the convection zone or the overshoot layer, the discontinuity is actually in the first (or second) derivative of the sound speed. However, if we consider the changes in sound speed for various solar models with differing depths of the convection zone, it is found that there is a sharp change in the sound-speed difference just below the depth of the shallower convection zone. We are effectively approximating this sharp change by a step function. Variations in the sound speed over length-scales comparable to or larger than the wavelength of the p-modes will not contribute to the oscillatory signal and

will only give rise to a smooth variation in the frequency. In models with overshoot, the acoustic cut-off frequency will have a term involving a delta function at the discontinuity; this has been neglected in our simplified treatment.

To a first approximation, the slow variation of k_r with radius can be taken into account by replacing $k_r r$ by $\int_r^{R_\odot} k_r \, dr$ in equations (2), (3) and (4). Thus, assuming ω_c and S_ℓ to be small compared to ω, equation (3) can be written as

$$\phi = -\frac{1}{2}\epsilon \int_{r_d}^{R_\odot} k_r \, dr + \frac{\epsilon}{4} \sin\left[2\omega\tau - \frac{\beta}{\omega} - \frac{\gamma \ell(\ell+1)}{\omega} + \psi\right], \qquad (5)$$

where

$$\tau = \int_{r_d}^{R_\odot} \frac{dr}{c}, \qquad \beta = \int_{r_d}^{R_\odot} \omega_c^2 \frac{dr}{c}, \qquad \gamma = \int_{r_d}^{R_\odot} \frac{c\, dr}{r^2}. \qquad (6)$$

Here the phase ψ is introduced to take care of the behaviour of k_r near the upper turning point where ω_c/ω is not small. In general, the quantity ψ itself could be a function of ω, but for simplicity we assume it to be a constant, since at least some of the ω dependence could be absorbed in the other terms.

From the definition of k_{r2}, we find that

$$\epsilon = \frac{\delta k_r^2}{k_r^2}, \qquad (7)$$

where δk_r^2 is the discontinuity in the wavenumber at $r = r_d$. The discontinuity in the wavenumber is due to two factors – the discontinuity in the sound speed, δc, at $r = r_d$, and the fact that the Brunt–Väisälä frequency, N, rises from a value close to zero in the convection zone and overshoot layer to a finite value immediately below $r = r_d$. Thus using

$$\omega_c^2 = \frac{g^2 \Gamma_1^2}{4c^2} \quad \text{and} \quad S_\ell^2 = \frac{c^2 \ell(\ell+1)}{r^2}, \qquad (8)$$

where g is the acceleration due to gravity and $\Gamma_1 = (\partial \ln P / \partial \ln \rho)_{ad}$, we get

$$\delta k_r^2 = -2\frac{\omega^2}{c^2}\frac{\delta c}{c} + \frac{g^2\Gamma_1^2}{c^4}\frac{\delta c}{c} + \frac{\ell(\ell+1)N^2}{r^2\omega^2}. \qquad (9)$$

Assuming that ω_c, S_ℓ and N are small relative to ω, and retaining the leading terms, we get

$$\epsilon \approx -2\frac{\delta c}{c} + \frac{1}{\omega^2}\frac{\delta c}{c}\left[\frac{g^2\Gamma_1^2}{2c^2} - \frac{2c^2\ell(\ell+1)}{r^2}\right] + \frac{\ell(\ell+1)N^2c^2}{r^2\omega^4}. \qquad (10)$$

Adopting the typical values of δc and N^2 from solar models, it can be seen that the first term makes the dominant contribution to ϵ. Further, ϵ, and hence the amplitude of the oscillatory component in the frequency, also depends on ℓ.

Thus from equation (4) we see that, to first order, the frequency can be written in the form

$$\nu_{n,\ell} = \frac{\omega_{n,\ell}}{2\pi} = \nu_s(n,\ell) - \frac{\epsilon}{4\tau_0}\sin\left[2\omega\tau - \frac{\beta}{\omega} - \frac{\gamma\ell(\ell+1)}{\omega} + \psi\right], \qquad (11)$$

where

$$\tau_0 = \int_{r_0}^{R_\odot} \frac{dr}{c}, \qquad (12)$$

$\nu_s(n,\ell)$ is the smooth component of the frequency, and ϵ is given by equation (10). It may be noted that this is a rather crude derivation of the oscillatory part, since the lower turning point r_0 itself will be a function of ℓ and n and, furthermore, other terms in k_r have also been neglected to replace the integral by τ_0 on the left-hand side of equation (4). The higher order terms in these approximations may introduce more terms in the amplitude, but these terms, which also depend on ℓ or ω, may be expected to be of the same form as those in equation (10). Thus this equation may serve as a good guide for choosing a functional form to be fitted to the frequencies in order to estimate the amplitude of the oscillatory component, and that is the only purpose for which it is used in the present study. A detailed analysis of the oscillatory contribution due to discontinuities in the derivatives of the sound speed has been carried out by Monteiro et al. (1994).

The oscillatory component in equation (11) is very small, with an amplitude of the order of a few hundredths to a few tenths of a μHz, while the smooth component is of the order of mHz. It is therefore difficult to filter out the oscillatory signal from the frequencies themselves. One way to extract this signal is to follow the suggestion by Gough (1990) and take the second difference of the observed frequencies. In the second difference, the oscillatory component will dominate over the smooth part and hence can be easily detected. The dominant component of the oscillatory part in equation (11) can be written as $A \sin(2\omega\tau)$. Further, for large n we can approximate $\omega = \omega_0 + \alpha n$, where ω_0 and α are constants. With these approximations, the second difference of equation (11) yields

$$\delta^2\nu = \delta^2\nu_s + 4A \sin^2(\tau\alpha)\sin(2\omega\tau). \qquad (13)$$

Thus the amplitude of the oscillatory component in the second difference is $4\sin^2(\tau\alpha) \approx 3.6$ times that in the frequency, while the smooth component may be expected to be diminished when differences are taken. Compared to this, the second derivative of the frequency is given by

$$\frac{d^2\nu}{dn^2} = \frac{d^2\nu_s}{dn^2} + 4A(\tau\alpha)^2\sin(2\omega\tau). \qquad (14)$$

Since $\tau\alpha \approx 2$, the two expressions have completely different amplitudes for the oscillatory component. This is to be expected, since the second difference cannot be expected to approximate the second derivative in such situations. Because of the inherent discretization in the frequencies, n is constrained to be an integer, and it is not possible to estimate the derivative to any reasonable accuracy using numerical values of the frequencies.

It may be noted that Monteiro et al. (1993a) estimate the second derivative using a cubic spline. Fig. 1 shows the second difference, as well as the second derivative computed using a cubic spline for $\ell = 5$ p-modes of a solar model. It is clear from the illustrations that the two estimates of the second derivative are completely at variance, and that the amplitude of the oscillatory component in the second deriva-

tive (using a cubic spline) is higher than that in the second difference, although not by the expected ratio between $d^2\nu/dn^2$ and $\delta^2\nu$. Neither of these estimates can be expected to approximate the true second derivative. Note that, in this figure, the smooth part of the frequency has not been removed. Further, it is also clear from this figure that the number of points for a single value of ℓ is not sufficient to define the oscillatory part uniquely. It is also difficult to separate the smooth and the oscillatory components in the frequency using only one value of ℓ. Consequently, it is highly desirable to combine the data for different values of ℓ.

Combination of modes with different values of ℓ is also difficult because the smooth part of the frequency has some ℓ dependence which is not very easy to eliminate in an unambiguous manner. It is found that this smooth part is rather small at larger frequencies ($\nu > 3.5$ mHz), but unfortunately the observations in this frequency range are not sufficiently accurate for any meaningful estimate of the small oscillatory signal. In order to overcome this problem, we take higher differences of the frequency, since in the higher differences the contribution due to the smooth part is decreased, while that due to the oscillatory component is enhanced. Moreover, most of the ℓ dependence in the smooth part is eliminated in the fourth difference, $\delta^4\nu$, which makes it possible to combine the data for different values of ℓ. If we consider the sixth difference, there is very little contribution from the smooth component, while in the eighth difference the smooth component is barely noticeable. As the order of the difference increases by two, the amplitude of the oscillatory component increases by a factor of $4\sin^2(\alpha\tau)$. However, the errors in observations also get enhanced in the higher differences. For example, if all the observed frequencies have the same standard deviation σ, then, assuming that the errors in different frequencies are uncorrelated, the corresponding variance in the second difference is $\approx 2.5\sigma$, while those in the fourth, sixth and eighth differences are $\approx 8.4\sigma$, 30.4σ and 113.4σ, respectively. Thus the variance increases by a factor of ≈ 12 in going from the second to the sixth difference, but then this increase is essentially compensated by a similar increase in the amplitude of oscillations. It may be noted that, since the oscillatory part of the frequency is not a pure sine function, the process of differencing will also introduce additional terms in the amplitude which depend on ℓ or ω. In this manner the form of amplitude given by equation (10) can serve only as a rough guide to the amplitude of the oscillatory part of the differences.

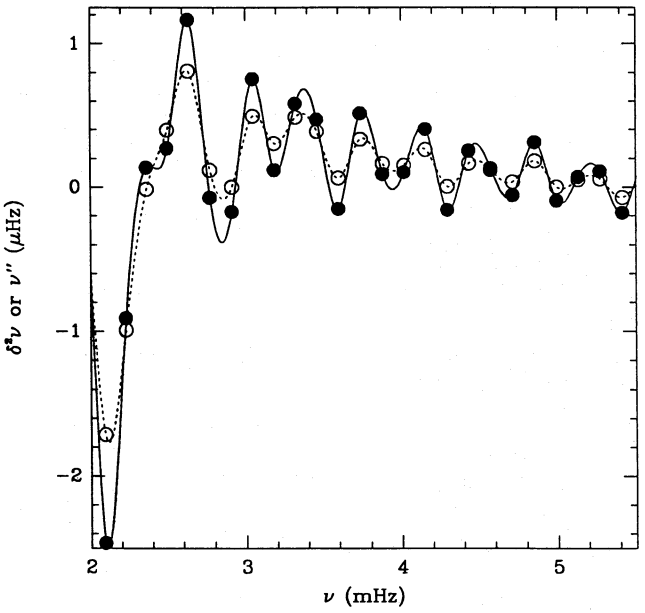

Figure 1. The second difference $\delta^2\nu$ and the second derivative (calculated using a cubic spline) of the frequency with respect to n as a function of the frequency ν for the degree $\ell = 5$ for model M1. The open and filled circles respectively mark the difference and the derivative. The dashed line is a cubic spline through the differences, while the solid line is a spline through the derivatives.

For the present study we have computed a series of models with varying extent of overshoot and depth of convection zone. For each of the models, we compute the frequencies $\nu_{n,\ell}$ for modes with $\ell \le 20$. The modes with higher degree ℓ are not very useful for this study since a large fraction of these modes either do not penetrate up to the base of the convection zone or have turning points close to that region and, as a result, are not affected by the discontinuity. In order to compute the amplitude of the oscillatory part, we combine the data for $5 \le \ell \le 20$ in the frequency interval 2–3.5 mHz and estimate the smooth part using a cubic spline data smoother, where the amount of smoothing can be controlled. The trend is removed until the residuals are symmetrically distributed about the frequency axis. The modes with $l < 5$ are ignored because the errors in the observed frequencies are too large for any reasonable estimate of the small oscillatory component. After the smooth component is removed we perform a least-squares fit to a function of a form similar to that of equation (11), that is

$$\delta^{2k}\nu_{\rm osc} = \delta^{2k}\nu - \delta^{2k}\nu_{\rm s} \qquad (15)$$
$$= \left[a_0 + \frac{a_1}{\nu_m^2} + \frac{a_2\ell(\ell+1)}{\nu_m^2} + \frac{a_3\ell(\ell+1)}{\nu_m^4}\right]\sin(2\nu_m\tau + \psi),$$

where

$$\nu_m = \nu - \frac{\gamma\ell(\ell+1)}{2\tau\nu}, \qquad (16)$$

and determine the coefficients a_0, a_1, a_2, a_3, τ, γ and ψ for $k = 1$, 2, 3 and 4. Hence $\nu_{\rm osc}$ is the oscillatory component of ν. The use of ν_m instead of ν eliminates the ℓ dependence of the argument of the sine term by a simple shift in frequencies. This allows us to plot the differences for all values of ℓ together, in order to check the fitted function against the frequencies. However, the ℓ dependence of the amplitude still remains. To eliminate this, instead of plotting $\delta^{2k}\nu_{\rm osc}$, we plot $\delta^{2k}\nu_{\rm osc} - \delta^{2k}\nu_\ell$, where

$$\delta^{2k}\nu_\ell = \ell(\ell+1)\left(\frac{a_2}{\nu_m^2} + \frac{a_3}{\nu_m^4}\right)\sin(2\nu_m\tau + \psi). \qquad (17)$$

This essentially transforms the amplitude for any given value of ℓ to the corresponding amplitude at $\ell = 0$. It may be noted that, in equation (15), we do not have the term corresponding to β/ν in equation (11). A change of the definition of ν_m, by subtracting a term of the form β/ν from the current expression, will merely yield an ℓ-independent shift in the

frequencies of all points. It is found that inclusion of this term does not improve the fit perceptibly and it is therefore ignored. As is clear from equation (15), the amplitude of the oscillatory term depends on ν; therefore, for the purpose of comparison, we use the average amplitude A in the given frequency interval $\nu_{m1} \leq \nu \leq \nu_{m2}$ given by

$$A = a_0 + \frac{a_1}{\nu_{m1}\,\nu_{m2}}. \tag{18}$$

While performing the fit, each point is weighted according to the quoted variance in the corresponding observed frequencies.

3 RESULTS

For the present work we have constructed 14 solar models with different extents of overshoot and depths of the convection zone to calibrate the amplitude of the oscillatory part in the frequency as a function of the extent of overshoot. The properties of these models are summarized in Table 1. In this table the extent of overshoot is quoted in terms of the pressure scaleheight H_p, which is assumed to be 56 000 km for all models. All these models have the correct solar radius and luminosity and use a non-local mixing length formulation as described by Antia, Chitre & Narasimha (1984). These models have been constructed by integrating the stellar structure equations from the outer boundary inwards. In order to satisfy the boundary conditions at the centre, the mixing length and a parameter determining the composition are adjusted. We achieved the latter by taking the hydrogen abundance profile to be the appropriate constant multiple λ (which is found to be close to unity) of the profile given by Bahcall et al. (1982), having fixed the heavy-element abundance at 0.018. Models M1–M6 have been computed using the OPAL opacities (Rogers & Iglesias 1992) with varying extent of overshoot, while models M7–M12 employ the opacity tables of Cox & Tabor (1976). The models M11 and M12 have been constructed using different values of the parameters C and D in the mixing length formulation (cf. Antia et al. 1984). For model M11 we use $C=1$ and $D=1$, and for model M12 we use $C=0.01$ and $D=0.1$, while all other models use $C=0.1$ and $D=0.01$. In all models the overshoot region is assumed to be adiabatically stratified. The last two models have been constructed using some artificial modifications to the OPAL opacities. Model M13 has been constructed by decreasing the opacity by 16.5 per cent near the base of the convection zone, to ensure an overshoot of $0.1H_p$ without changing the depth of the adiabatic layer. For this model the opacity was taken as

$$\kappa = \begin{cases} \kappa_o \dfrac{1+0.165(r/\mathrm{R}_\odot - 0.72069)/0.00632}{1.165} \\ \quad \text{if } 0.72701 > r/\mathrm{R}_\odot > 0.72069, \\ \kappa_o \dfrac{1}{1.165} \\ \quad \text{if } 0.72069 \geq r/\mathrm{R}_\odot \geq 0.70459, \\ \kappa_o \dfrac{1+0.165(0.70459 - r/\mathrm{R}_\odot)/0.04310}{1.165} \\ \quad \text{if } 0.70459 > r/\mathrm{R}_\odot > 0.66149, \\ \kappa_o \\ \quad \text{otherwise,} \end{cases} \tag{19}$$

where κ_o is the opacity computed by interpolating in the opacity tables of Rogers & Iglesias (1992). Model M14 has been constructed by decreasing the opacity uniformly by 10 per cent, while the composition is adjusted to match the boundary conditions at the centre. Because of these constraints, there is not much difference between this model and model M1.

Fig. 2 shows the temperature gradient $\nabla = \mathrm{d}\log T/\mathrm{d}\log P$ as a function of radial distance in the solar models M7–M10. For the model M7, which has no overshoot, the temperature gradient is continuous, but its derivative is discontinuous at

Table 1. Properties of solar models.

Model	$r_d/R_\odot$	Extent of overshoot	τ (sec)	γ (mHz)	Opacity
M1	0.7124	$0.00H_p$	2102	0.01367	OPAL
M2	0.7040	$0.10H_p$	2125	0.01448	OPAL
M3	0.6958	$0.20H_p$	2150	0.01537	OPAL
M4	0.6874	$0.30H_p$	2176	0.01632	OPAL
M5	0.6784	$0.40H_p$	2201	0.01736	OPAL
M6	0.6702	$0.50H_p$	2224	0.01837	OPAL
M7	0.7220	$0.00H_p$	2068	0.01270	CT
M8	0.7125	$0.12H_p$	2098	0.01362	CT
M9	0.6981	$0.29H_p$	2142	0.01512	CT
M10	0.6838	$0.45H_p$	2185	0.01674	CT
M11	0.7224	$0.00H_p$	2070	0.01266	CT
M12	0.6968	$0.00H_p$	2155	0.01526	CT
M13	0.7126	$0.10H_p$	2100	0.01361	Eq. (19)
M14	0.7108	$0.00H_p$	2105	0.01382	$0.9 * \kappa_{\mathrm{OPAL}}$

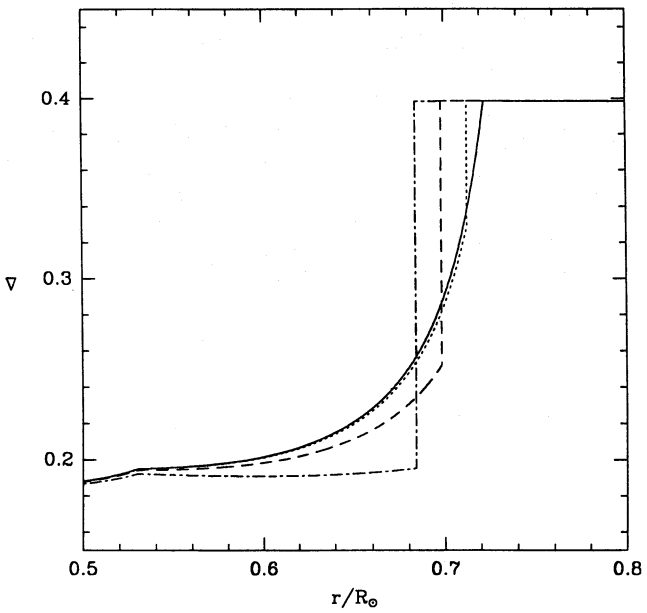

Figure 2. The temperature gradient $\nabla = \mathrm{d} \log T / \mathrm{d} \log P$ as a function of radial distance for the solar models M7–M10. The solid line is the gradient for model M7, the dotted line is for model M8, the dashed line is for model M9, and the dot-dashed line is the gradient for model M10.

the base of the convection zone. For models M8–M10, which have some overshoot, the temperature gradient itself is discontinuous at the base of the overshoot layer. Further, the magnitude of the discontinuity increases with the extent of overshoot. In Fig. 3 we show the difference in the sound speed relative to the sound speed in model M1 as a function of radial distance. Model M1 has no overshoot, and hence the sound-speed profile should be relatively smooth. Thus the sharp change in the sound speed for models with overshoot is very clearly discerned when compared with that in model M1. Use of this figure can justify our assumption of a discontinuity in the sound speed at the base of the convection zone, which we used to obtain a simple expression for the oscillatory component of the frequencies. It can be seen that the fall in $\delta c/c$ towards the centre is more gradual and can be considered as a smooth variation. It is clear from the figure that the jump in sound speed at the bottom of the overshoot layer increases with an increase in the extent of overshoot; for example, for model M3, $\delta c/c$ relative to model M1 is around 0.004, while for model M6 $\delta c/c$ is around 0.02. The extent of overshoot in model M6 is 2.5 times that in model M3. Further, it can be seen that the sound-speed profiles in models M1 and M14 and models M7 and M11 are very similar.

For a representative value of $\delta c/c$, the magnitude of the oscillatory component in the frequencies can be estimated using equations (11) and (10). For example, if we take typical values of the physical quantities involved, that is, the radial distance of the base of the convection zone $r_\mathrm{d} \approx 5 \times 10^{10}$ cm, the sound speed $c \approx 2.2 \times 10^7$ cm s^{-1}, the adiabatic index $\Gamma_1 \approx 1.66$, the acceleration due to gravity $g \approx 5.3 \times 10^4$ cm s^{-2}, the Brunt–Väisälä frequency $N/2\pi \approx 0.2$ mHz and $\tau_0 \approx 3500$ s (corresponding to $r_0 = 0$), then the amplitude of the oscillatory component is about 0.4 μHz for $\delta c/c \approx 0.02$, which is a reasonable estimate for the model M6. Although, in the present work, we have avoided estimating the amplitude of the oscillatory component in the frequencies directly, for the sake of comparison we attempted an estimate of the amplitude for the model M6 and found it to be about 0.11 μHz. It is clear that the crude model considered in Section 2 gives the ampitude to within an order of magnitude of the actual value. Since, in this paper, we are interested only in the functional form of the amplitude that can be used to fit the oscillatory part of the exact frequencies, this simple analysis should be sufficient. For other models, the amplitude of oscillations in the frequency is expected to be much less, and it is therefore desirable to amplify the oscillations by taking higher differences. Another problem in dealing directly with the frequencies is that, for each ℓ, there are not enough points to be able to separate out the smooth part in the frequency from the oscillatory part in an objective and unambiguous manner. The final amplitude depends to some degree on the extent to which the smooth part is removed. This is particularly true for observations where the median value of the standard deviation is comparable to or larger than the amplitude of the oscillatory component.

For fitting the function to the second difference of the frequencies, we choose a frequency range of 2.5–3.8 mHz. We do not consider lower frequencies because of the very pronounced non-oscillatory trend in $\delta^2\nu$ for frequencies below ≈ 2.5 mHz, which is difficult to eliminate. This trend can be seen very clearly in Fig. 1. Frequencies higher than 3.8 mHz are not considered because the observed frequencies in this range have rather large errors. Before combining the data for all values of ℓ, it is necessary to remove the smooth part in the second difference, because the smooth component itself has significant ℓ dependence, as can be seen from Fig. 4(d), which shows the second differences for model M1. It is clear that the smooth component for points with $5 \le \ell \le 10$, which are marked by crosses, is different from that for $16 \le \ell \le 20$, indicated by filled squares. Consequently, we divide the second differences of the frequencies $\delta^2\nu$ into three groups corresponding to $5 \le \ell \le 10$, $11 \le \ell \le 15$ and $16 \le \ell \le 20$. For each group we filter out the smooth trend separately. The residuals after the smooth trend has been removed are combined, and the function given by equation (15) is then fitted to the combined data. Of course, there will be some ℓ dependence in the smooth part within each subgroup also, but consideration of individual values of ℓ separately is rather difficult since the number of points for each ℓ is too small to separate out the smooth part unambiguously. It is preferable to combine the data after removing the smooth part independently, since otherwise the number of points in each range is limited. This introduces significant uncertainties in the fitting process, particularly in the presence of errors. In Fig. 4(e), which shows the residuals after the smooth part has been removed, the oscillations are barely noticeable. After introducing the ℓ-dependent shift to the abscissae defined by equation (16), the oscillations are very clear (cf. Fig. 4f). The same procedure was followed for the observed solar frequencies also. Figs 4(c) and (f) show, respectively, the results of the fits to observations and to frequencies computed for model M1. It can be seen that there is some difficulty in removing the smooth component for the observations, and the three curves in Fig. 4(a) show some variation in form which is probably not expected, as can be seen from Fig. 4(d) which displays the same curves for model M1.

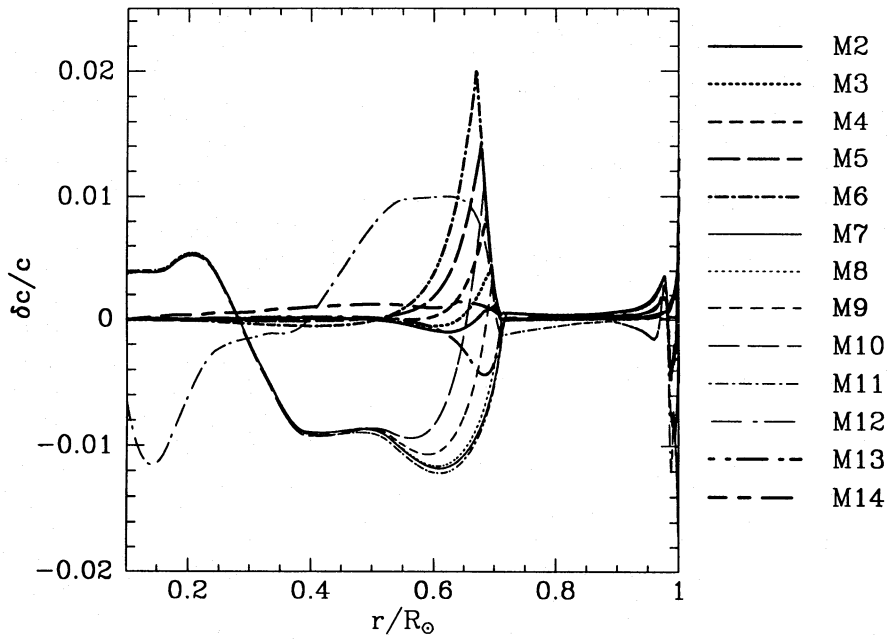

Figure 3. The relative sound speed difference $\delta c/c$ between the models M2–M14 and M1 is shown as a function of radius. The models using OPAL opacities are represented by heavy lines.

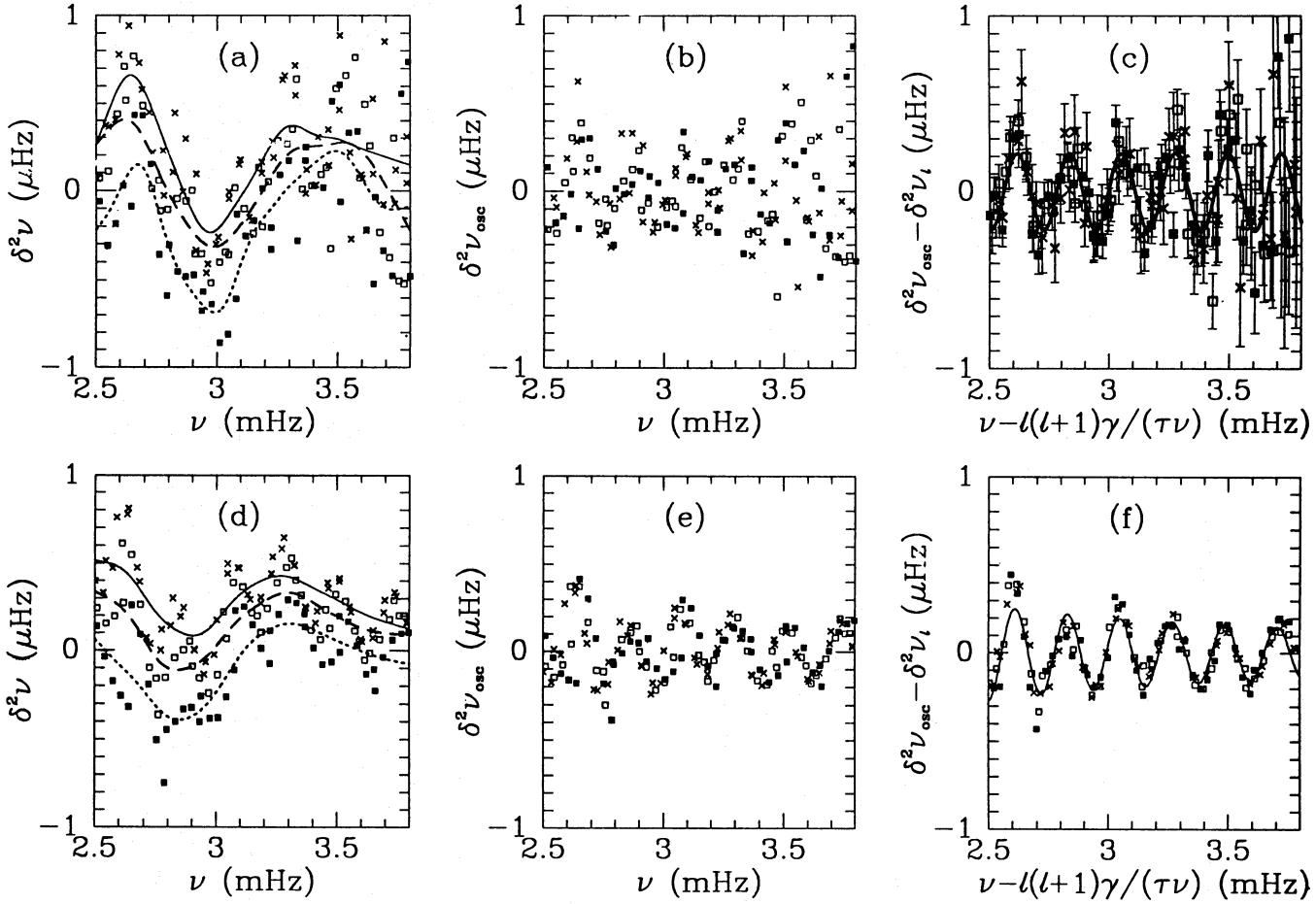

Figure 4. The second difference $\delta^2\nu$ for $5\leq\ell\leq20$ and frequency ν in the range 2.5–3.8 mHz for the observed frequencies and the frequencies computed for model M1. (a) and (d) show the differences for the observations and the model, respectively. The points for $5\leq\ell\leq10$ are marked by crosses, those for $11\leq\ell\leq15$ by open squares, and those for $16\leq\ell\leq20$ by filled squares. The non-oscillatory part is represented by a solid curve for $5\leq\ell\leq10$, a dashed curve for $11\leq\ell\leq15$ and a dotted curve for $16\leq\ell\leq20$. The residuals after subtracting the smooth trend, as represented by the lines, are plotted in (b) for the observations and in (e) for the model. (c) shows the result of the fit to the observations plotted after removing the ℓ dependence of the differences. Similarly, (f) is the fit for model M1.

For the second differences, we thus find that it is very difficult to remove the smooth trend in the frequencies in an unambiguous manner. The fact that the set of frequencies has to be divided into three groups makes the situation even worse, since the number of points decreases in the process. Besides, we cannot be quite sure that the smooth part has been removed to the same extent in each ℓ group. The difficulties can be gauged from Fig. 4(f) where it can be seen that, even for the frequencies computed from the model, the fit is far from perfect. As a result, we have looked into higher differences of the frequencies. For the fourth and sixth differences of the frequencies, we find that there is no perceptible ℓ dependence in the smooth part and hence the differences for all ℓ values in the range 5–20 can be combined even before the smooth trend is removed. This makes the task of removing the smooth trend easier, as the number of points we are now dealing with is larger, about 170. Besides, of course, the higher differences have the advantage that the oscillations are magnified further while the smooth part is reduced. Thus the oscillatory part can be extracted quite unambiguously from the smooth background. For these differences we can use a slightly lower frequency range, since the pronounced non-oscillatory trend seen in the second difference is significantly reduced. Consequently, we have chosen the range $2.0 \le \nu \le 3.5$ mHz for both $\delta^4\nu$ and $\delta^6\nu$. A shift in the range of frequencies used enables us to use more accurate data from observations at low frequencies.

The results of the fits to the fourth difference of the observed solar frequencies, and to the fourth difference of the frequencies computed for model M1 as a representative model, are shown in Fig. 5. It can be seen that the oscillatory part is well defined and can be extracted very easily. The fit to the oscillations in the frequencies computed from the models is almost perfect, which justifies the functional form of the amplitude given by equation (15). It can be seen from Fig. 5 that the 'smooth' component in the frequencies is also oscillatory, but with a larger wavelength. In fact, this component can be identified as the oscillatory signature due to the second helium ionization zone (Roxburgh & Vorontsov 1993). Since this ionization zone occurs at a shallower acoustic depth, the wavelength of the oscillatory component is larger, and when we take higher differences the smaller wavelength oscillatory component due to the discontinuity at the base of the convection zone dominates. Fig. 6 shows the fits to the sixth difference of the observed solar frequencies and the frequencies computed for model M1. As can be seen from the figure, the smooth component of the frequency is further reduced.

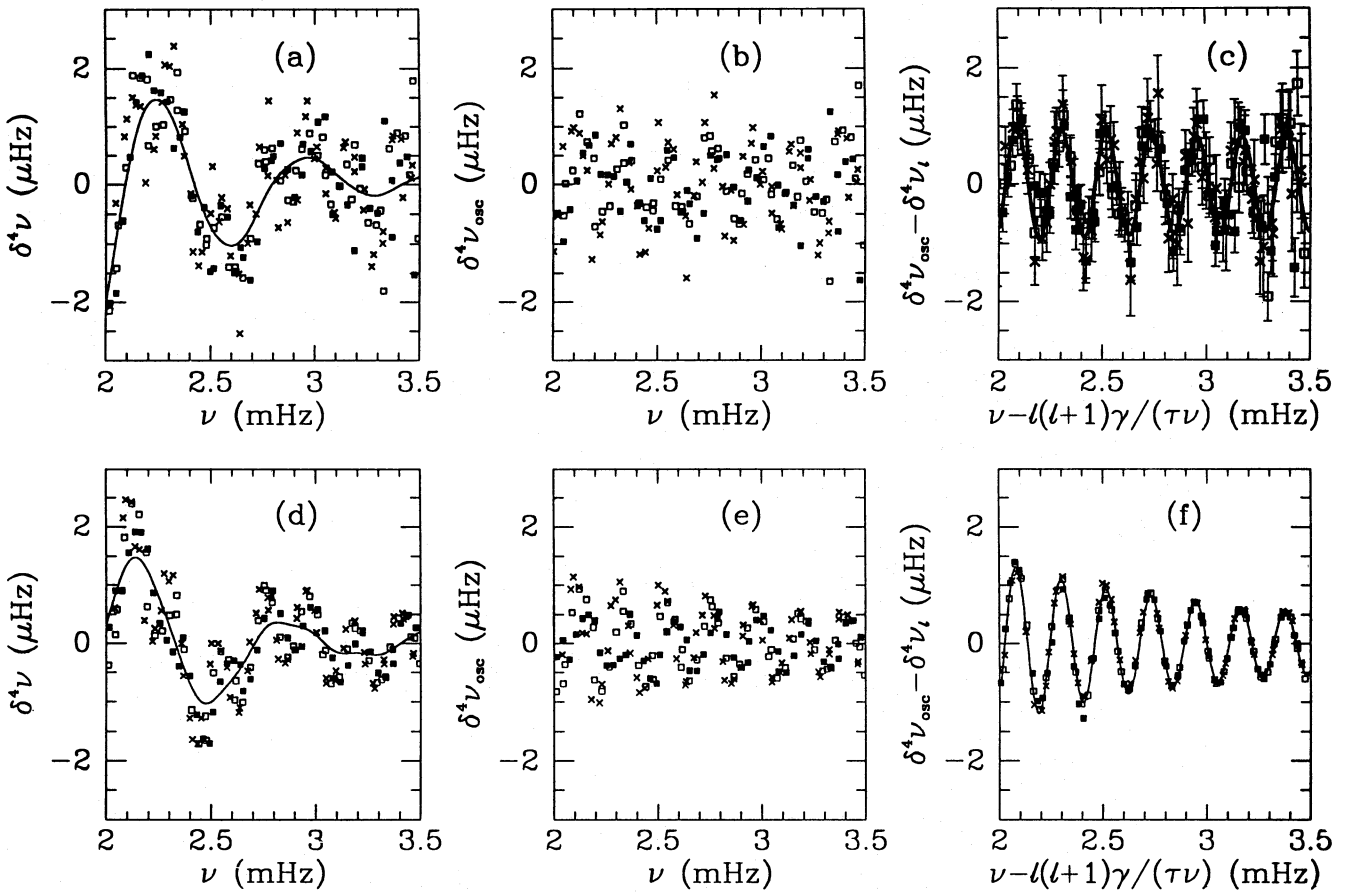

Figure 5. The fourth difference $\delta^4\nu$ for $5 \le \ell \le 20$ and frequency ν in the range 2.0–3.5 mHz for the observed frequencies and the frequencies computed for model M1. (a) and (d) show the differences for the observations and the model, respectively. The different symbols have the same meanings as in Fig. 4. The non-oscillatory part is represented by the solid curve. The residuals, after subtracting the smooth trend as represented by the line, are plotted in (b) for the observations and in (e) for the model. (c) shows the result of the fit to the observations plotted after removing the ℓ dependence of the differences. Similarly, (f) is the fit for model M1.

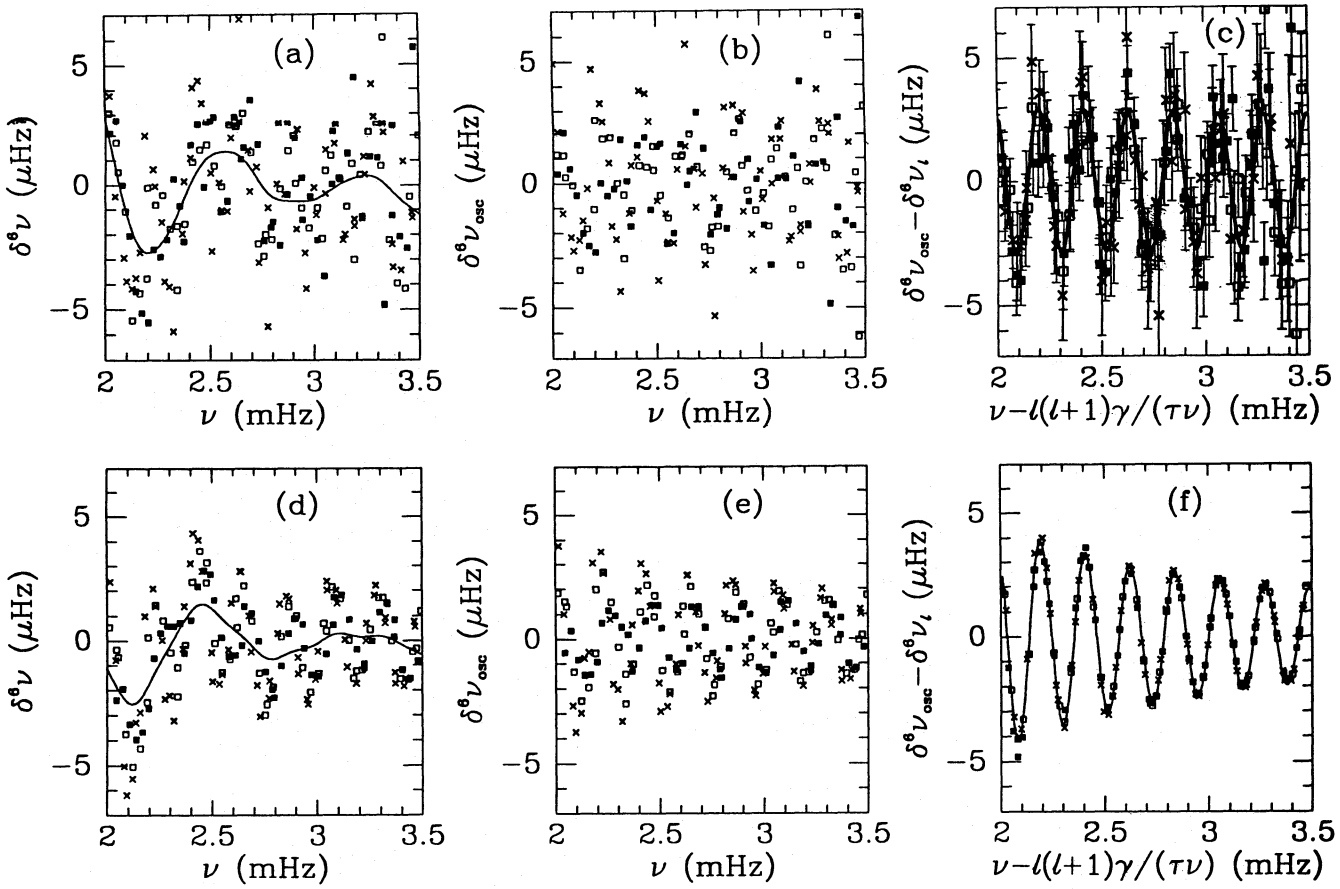

Figure 6. The same as Fig. 5, but for the sixth difference $\delta^6\nu$ of the frequencies.

In order to demonstrate the ℓ dependence of the amplitude, we take the oscillatory component of the fourth difference for model M1 as shown in Fig. 5(e) and perform separate fits for different ranges of ℓ. In this case we drop the ℓ-dependent terms in the fitting function given in equation (15), by setting $a_2 = a_3 = 0$, and use five sets of ℓ values, namely {5, 6, 7}, {8, 9, 10}, {11, 12, 13}, {14, 15, 16} and {17, 18, 19}. For each of these ℓ ranges we estimate the amplitude of the oscillatory component, and the results are shown in Fig. 7, where the amplitudes are plotted against $\ell(\ell+1)$ for the middle value of ℓ in the corresponding range. The least-squares fit to a straight line is shown by the solid line. It is clear that the amplitude is decreasing almost linearly with $\ell(\ell+1)$. It may be noted that, since the number of points in each subgroup of ℓ values is rather small, the amplitude cannot be determined very accurately.

Encouraged by the fact that the fourth and sixth differences made the oscillations in the frequencies stand out clearly without being overwhelmed by observational errors, we went one step further and decided to examine the eighth difference of the frequencies. We find that, for the eighth difference, the smooth component of the frequency is barely noticeable and hence we can fit the function of the form given in equation (15) directly to the differences. Fig. 8 shows the fits to the observations and the frequencies computed for models M1 and M2.

In order to estimate the amplitude of the oscillatory component in the solar frequencies, the same treatment is applied to the observed data of Libbrecht et al. (1990). In this case, however, apart from the coefficients, we also need to estimate the associated uncertainties arising from the observational errors. The errors in the computed amplitude

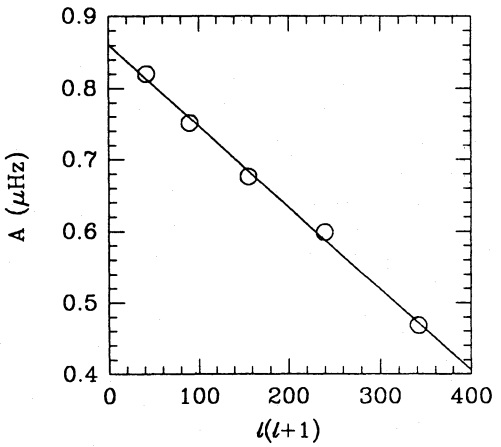

Figure 7. The amplitude of the oscillatory component of the fourth difference of the frequency for model M1 as a function of $\ell(\ell+1)$ in the frequency range $2.0 \le \nu \le 3.5$ mHz. Each point represents the amplitude obtained for frequencies using modes with $\ell-1$, ℓ and $\ell+1$. The solid line gives the least-squares fit to a straight line for these points.

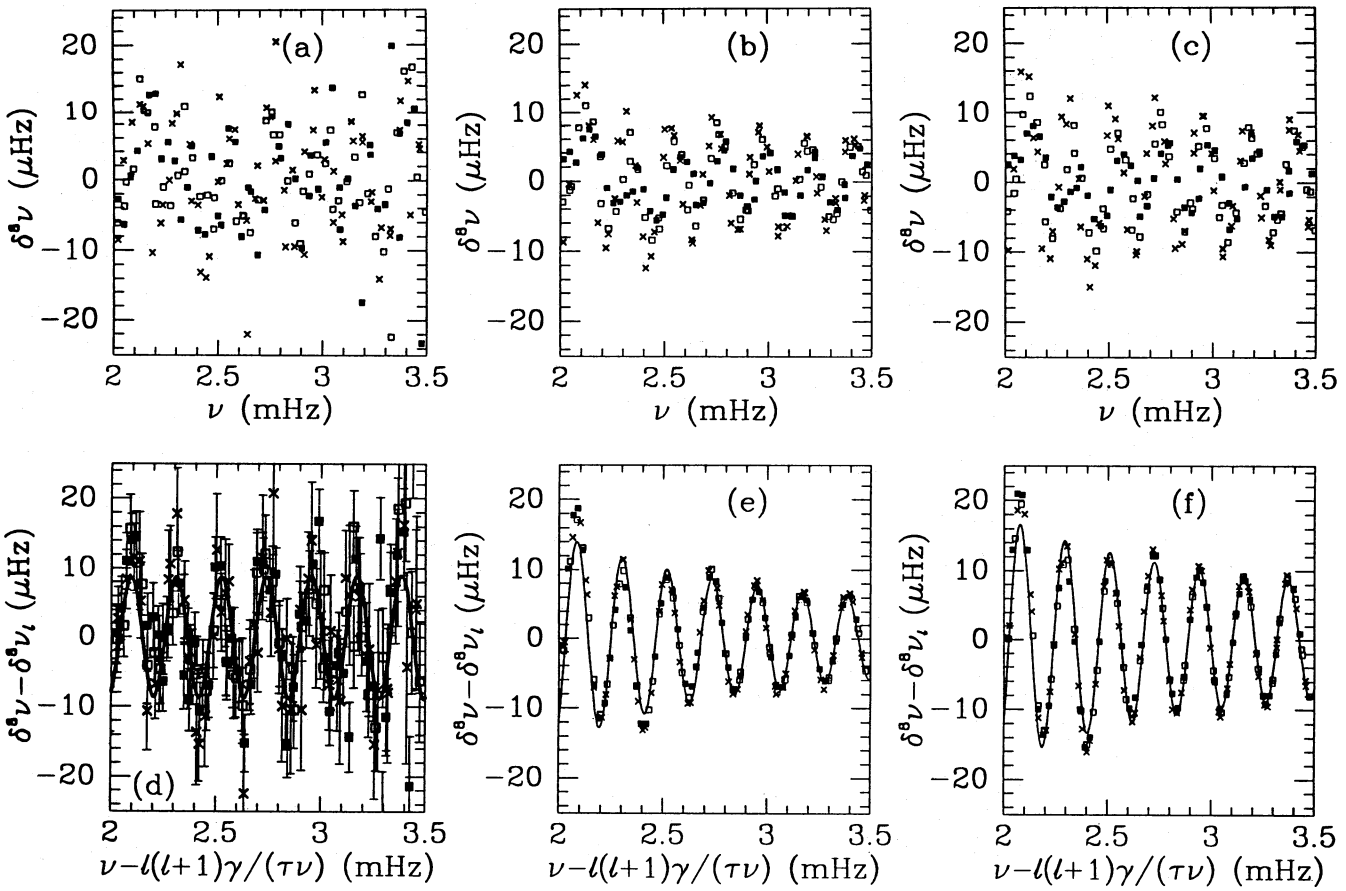

Figure 8. The eighth difference $\delta^8\nu$ for $5 \le \ell \le 20$ and frequency ν in the range 2.0–3.5 mHz of the observed frequencies and the frequencies computed for the models M1 and M2 are shown in (a), (b) and (c) respectively. The different symbols have the same meanings as in Fig. 4. (d), (e) and (f) show the fits to the differences for the observations, model M1, and model M2, respectively, after removing the ℓ dependence.

and τ were estimated by performing a simulation using artificially generated data sets. The simulated data were generated by adding random errors, with standard deviation as quoted by the observers, to the computed frequencies of model M1. For each set of simulated data, the amplitude was computed in the same way as for the models. From the distribution of amplitudes in a set of 20 simulations we have estimated the mean value and the variance. The standard deviation and the mean value of the amplitude, τ and γ, as estimated by the simulations for various differences, are listed in Table 2, which also gives the corresponding values obtained for model M1 (without adding errors). It can be seen that in all cases the mean values from simulations are close to the actual value for the model. To check if it is adequate to use results of the simulations based on the computed frequencies of model M1 only, we have produced 20 sets of simulated data for each model and tried to see, for the eighth difference of the frequencies, how the results compare. From the results shown in Table 3 it is clear that the variances of the parameters computed from the different models are not very different. In fact, the variance computed from simulations on model M1 is one of the highest, which is only to be expected as model M1 has about the lowest amplitude. Thus, by using the variance of parameters obtained from model M1, we will not in any way be underestimating the errors in the least-squares fit.

In principle, it is possible to consider still higher order differences to amplify the signal; however, the growth in the errors will make such an exercise quite meaningless. The errors in the computed differences can be estimated from the quoted errors in the observed frequencies by assuming that these errors are uncorrelated. In Table 4 we show the median of the errors, as well as the minimum value of the error for each set of differences. We also list the amplitudes obtained for model M1, which is among the models that give the lowest amplitudes, and appears to be the closest to observations. The amplitudes obtained from observed solar frequencies are also listed. From Table 4, it can be seen that, for all differences, the estimated variance in the amplitude is about 0.26 times the median value of the error in observed values. Table 4 also gives the ratios of the amplitudes obtained to the median error. It can be seen from this table that the results are most promising for the fourth difference. The ratio of the amplitude to the error is lower for the sixth difference and lower still for the eighth. We do not therefore think it worthwhile to consider higher differences. It may be noted that the ratio of the amplitudes for the sixth and fourth differences, as well as that of the eighth and sixth differences, is consistent with our crude estimate of 4 $\sin^2(\alpha\tau)$ in Section 2. It may also be noted that for the second difference we have used a slightly different frequency range and, as a result, the ratio of amplitudes for $\delta^2\nu$ and $\delta^4\nu$ is slightly different.

Table 2. Variance of computed parameters.

Difference	Results of Model M1			Mean Results From Simulations			Variance of Computed Quantities		
	A (μHz)	τ (sec)	γ (mHz)	A (μHz)	τ (sec)	γ (mHz)	σ_A (μHz)	σ_τ (sec)	σ_γ (mHz)
$\delta^2\nu$	0.196	2283	0.0166	0.171	2281	0.0177	0.042	28	0.0024
$\delta^4\nu$	0.852	2318	0.0144	0.849	2315	0.0149	0.105	15	0.0024
$\delta^6\nu$	2.822	2319	0.0143	2.864	2316	0.0145	0.378	17	0.0025
$\delta^8\nu$	9.252	2308	0.0125	9.207	2304	0.0131	1.441	22	0.0044

Table 3. The fitted coefficients for the eighth difference.

Model	Results From Models			Mean Results From Simulations			Variance of Computed Quantities		
	A (μHz)	τ (sec)	γ (mHz)	A (μHz)	τ (sec)	γ (mHz)	σ_A (μHz)	σ_τ (sec)	σ_γ (mHz)
M1	9.252	2308	0.0125	9.207	2304	0.0131	1.441	22	0.0044
M2	11.734	2320	0.0131	11.743	2320	0.0136	1.388	17	0.0027
M3	15.956	2345	0.0138	15.821	2347	0.0144	1.109	12	0.0014
M4	18.999	2371	0.0144	18.999	2374	0.0146	1.197	10	0.0011
M5	20.778	2400	0.0155	20.907	2403	0.0153	1.132	10	0.0013
M6	21.639	2429	0.0169	21.709	2429	0.0167	0.848	10	0.0014
M7	11.441	2283	0.0128	11.483	2274	0.0117	1.672	21	0.0029
M8	14.983	2295	0.0127	14.974	2290	0.0122	1.597	15	0.0020
M9	21.515	2338	0.0136	21.367	2340	0.0140	1.206	9	0.0012
M10	25.294	2383	0.0148	25.298	2386	0.0149	1.201	8	0.0008
M11	11.114	2304	0.0127	11.087	2293	0.0115	1.657	21	0.0030
M12	9.096	2364	0.0143	9.100	2366	0.0145	1.315	26	0.0030
M13	13.208	2303	0.0130	13.141	2295	0.0122	1.539	18	0.0024
M14	9.415	2311	0.0124	9.271	2306	0.0123	1.521	26	0.0043

Table 4. Comparison of errors in various differences.

Difference	Errors in obs.		Amplitude			$\frac{\text{Ampl.}}{\text{Med. Error}}$		$\frac{\sigma_A}{\text{Med. Error}}$
	Median (μHz)	Min. (μHz)	M1 (μHz)	Obs. (μHz)	(σ_A) (μHz)	M1	Obs.	
$\delta^0\nu$	0.060	0.030	0.037	0.032	0.010	0.617	0.533	0.167
$\delta^2\nu$	0.141	0.082	0.196	0.218	0.042	1.390	1.546	0.298
$\delta^4\nu$	0.402	0.220	0.852	0.860	0.105	2.119	2.142	0.261
$\delta^6\nu$	1.459	0.813	2.822	2.801	0.378	1.934	1.920	0.259
$\delta^8\nu$	5.428	3.148	9.252	8.797	1.441	1.704	1.621	0.265

In order to compare observations against the models, we have plotted the amplitude against τ for various models and observations for each of the differences considered. Table 5 shows the ratio of amplitudes for models M2–M14 relative to that of model M1, for all the differences considered. The amplitude is essentially a function of the extent of the overshoot. However, τ, which is basically the acoustic depth of the base of the overshoot layer, depends on the depth of the discontinuity, that is, the extent of the convection zone and the overshoot layer. As a result, models with the same extent of overshoot but with different depths of the base of the convection zone will give different values of τ. There is also some remnant ambiguity due to the fact that, for a given extent of overshoot, the amplitude depends on the opacity used, since the extent of discontinuity in the temperature gradient is controlled by the opacity gradient. Thus in the two-dimensional τ–A graph we expect that the models will be well separated. Fig. 9 shows our results for all the differences considered in the present work, that is, the second difference $\delta^2\nu$, the fourth difference $\delta^4\nu$, the sixth difference

Table 5. Amplitude ratios for solar models.

Model	$\delta^2\nu$	$\delta^4\nu$	$\delta^6\nu$	$\delta^8\nu$	$\delta^4\nu$	$\delta^4\nu$
	$5 \le \ell \le 20$	$5 \le \ell \le 20$	$5 \le \ell \le 20$	$5 \le \ell \le 20$	$5 \le \ell \le 20$	$0 \le \ell \le 4$
	2.5–3.8 mHz	2.0–3.5 mHz	2.0–3.5 mHz	2.0–3.5 mHz	3.5–5.5 mHz	2.0–5.0 mHz
M1	1.000	1.000	1.000	1.000	1.000	1.000
M2	1.284	1.317	1.279	1.268	1.517	1.333
M3	1.971	1.882	1.787	1.725	2.526	2.019
M4	2.637	2.312	2.157	2.053	3.390	2.597
M5	3.082	2.691	2.404	2.246	3.893	3.094
M6	3.423	2.959	2.575	2.339	4.367	3.574
M7	1.056	1.123	1.202	1.236	1.154	1.192
M8	1.542	1.543	1.592	1.619	2.067	1.795
M9	2.790	2.504	2.408	2.325	3.671	2.852
M10	3.612	3.180	2.907	2.734	4.710	3.629
M11	1.033	1.133	1.179	1.201	1.154	1.174
M12	1.016	0.975	0.938	0.983	1.007	0.989
M13	1.388	1.393	1.414	1.427	1.801	1.547
M14	1.019	1.010	1.010	1.018	0.992	0.949
Obs.	1.110	1.010	0.992	0.951	–	–

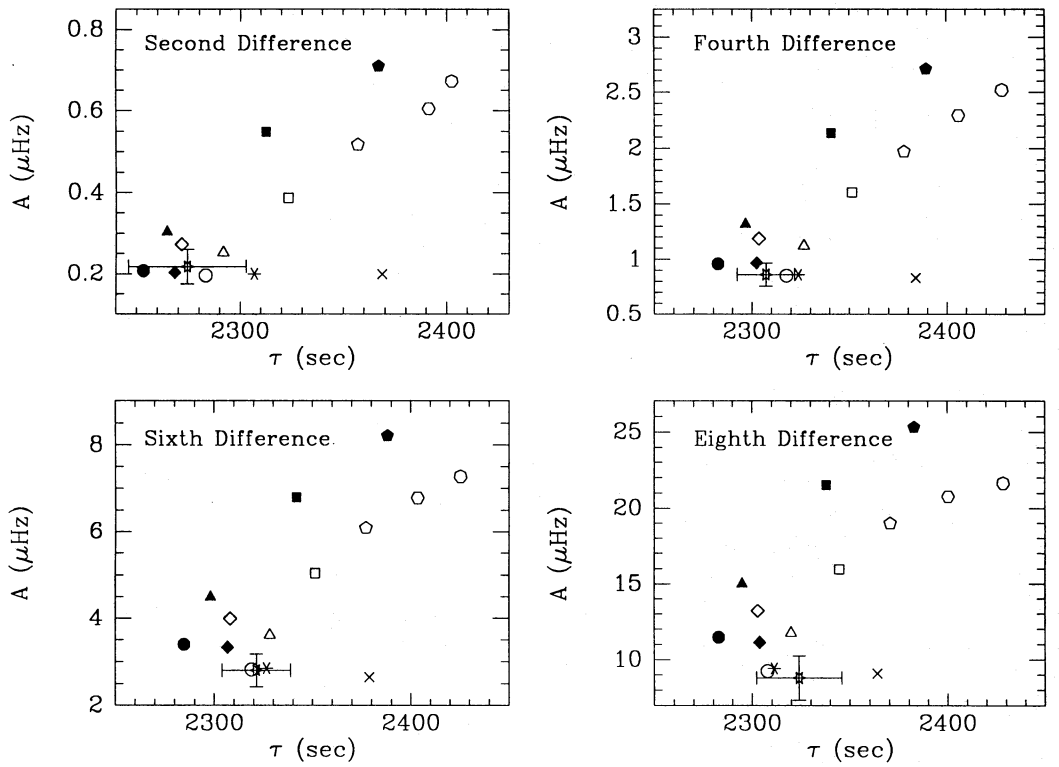

Figure 9. The amplitude A and the acoustic depth τ of the discontinuity for the different models for various differences are shown in the four figures. The different symbols are as follows: open circle (model M1), open triangle (M2), open square (M3), open pentagon (M4), open hexagon (M5), open heptagon (M6), filled circle (M7), filled triangle (M8), filled square (M9), filled pentagon (M10), filled diamond (M11), cross (M12), open diamond (M13) and asterisk (M14). The star with error bars represents the result for the observed frequencies.

$\delta^6\nu$ and the eighth difference $\delta^8\nu$. It can be seen that models M7–M10 constructed with the Cox & Tabor (1976) opacities show higher oscillation amplitudes than those constructed with the OPAL opacities with a similar extent of overshoot. This may be expected, since the opacity gradient at the base of the convection zone is lower in models constructed using OPAL opacities: for example, for model M1 the opacity scaleheight at the base of the convection zone is 6.22×10^4 km, while for model M7 it is 5.21×10^4 km. Since the radiative gradient ∇_R is essentially determined by opacity,

its gradient also varies with the opacity gradient. From equation (10) it can be seen that the amplitude is expected to be proportional to $\delta c/c$. For solar models it may be expected that the difference δc arises because of the departure of the temperature gradient from its adiabatic value. Thus to first order

$$\frac{\delta c}{c}=\frac{1}{2}\frac{\delta T}{T}=\frac{1}{2H_p}\delta\nabla\delta r=\frac{1}{2H_p}\frac{\mathrm{d}\nabla}{\mathrm{d}r}(\delta r)^2, \tag{20}$$

where δr is the distance from the base of the convection zone. Now the quantity $(1/2H_p)/\mathrm{d}\nabla/\mathrm{d}r$ is 0.92×10^{-10} km^{-2}, 1.06×10^{-10} km^{-2} and 0.92×10^{-10} km^{-2} for models M1, M7 and M12, respectively. Thus we can expect the amplitudes for model M7 to be about 15 per cent higher than those for models M1 and M12. Further, the amplitudes of models M1 and M12 should be nearly equal. This is consistent with the results in Table 5. Thus, apart from the extent of overshoot, the amplitudes also depend on the opacity gradient at the base of the convection zone, and also on any other possible force field (e.g. magnetic field) present near the base of the convection zone.

In the presence of a magnetic field the dispersion relation for the acoustic waves will be modified to $\omega^2\approx k^2(c^2+v_a^2)$, where v_a is the Alfvén speed. Hence the presence of a localized magnetic field near the base of the convection zone can also lead to a discontinuity in the wavenumber k. In this case

$$\epsilon=\frac{\delta k^2}{k^2}=-\frac{v_a^2}{c^2}=-\frac{B^2}{4\pi\Gamma_1 P}, \tag{21}$$

where P is the gas pressure and B is the strength of the magnetic field. Thus a magnetic field of 10^6 G will yield $\epsilon=0.0008$, which gives an amplitude of 0.009 μHz in the frequencies. Further, it should be noted that in equation (10) $\delta c/c<0$, since the temperature gradient reduces sharply below the convection zone. Thus the sign of the contribution of a magnetic field due to ϵ is opposite to that due to δc, and in principle it is possible to reduce the amplitude of the oscillatory component in the frequency by invoking a few-megagauss magnetic field below the base of the convection zone.

The acoustic depth of the discontinuity, τ, for the models constructed using Cox & Tabor opacities is lower than for the corresponding models constructed using OPAL opacities. This is expected since the convection zone depth is slightly smaller for models with Cox & Tabor opacities (Table 1). It may be noted that the value of τ computed by the least-squares fit is always slightly higher than the actual value given by equation (6), for all models (cf. Table 1). This is a consequence of the phase ψ in the sine term having a component proportional to the frequency (Monteiro et al. 1993b), which gets absorbed in τ during the fitting process. As a result, it is not possible to estimate the acoustic depth τ using this technique, but it may be possible to distinguish between models with different τ.

It is interesting to note that all the four figures appear to be rather similar except for the fact that the amplitude scales are different in each case. This shows that the uncertainties in the fitting procedure are probably not very significant. From Table 5 it can be seen that the relative amplitudes of the oscillatory part are essentially independent of the difference, though there is some variation arising mainly due to the fact that the factor $4\sin(\tau\alpha)$, which is introduced in going to higher differences, depends on τ. As a result, for models with high overshoot the relative amplitude decreases slowly with increasing order of difference.

The results for the observed frequencies are shown with error bars which correspond to the variance of the parameters obtained from the simulations. It can be seen that the results consistently point to the fact that, of all the models, model M1 is closest to the actual Sun. Note that model M1 has no overshoot and the depth of the convection zone in this model is the same as that inferred for the Sun by Christensen-Dalsgaard, Gough & Thompson (1991). All the figures indicate that the observed solar frequencies are consistent with a model without overshoot. It can be seen that the error bars are significantly larger for the second difference, which reflects the uncertainties in extracting the oscillatory part and performing the least-squares fit. In view of the errors on the fitted parameters, neglecting systematic errors due to uncertainties in opacity, we can put a 2σ upper limit of $0.1H_p$ on the extent of overshoot at the base of the solar convection zone.

We find that if a higher frequency range, like $3.5\le\nu\le5.5$ mHz, is considered, even for the fourth difference, no smooth part of the frequencies has to be removed. This can be seen from Fig. 10, where we show the fit to the fourth difference of the frequencies computed for model M1, while the $A-\tau$ diagram displaying results for all the models is shown in Fig. 11(a). Thus the uncertainty due to removal of the smooth part of the frequency should be reduced in this case. Further, since most of the terms in the oscillatory part fall off as $1/\omega^2$ or faster, the oscillatory part can be extracted relatively easily. In fact, the sinusoidal oscillations are apparent in Fig. 10(a) even before the ℓ-dependent shifts in the frequency and amplitude are corrected for. This frequency range is not, however, very useful for the solar case, as the observed frequencies in this range have large errors. Another disadvantage with this range is that, since the amplitude is a decreasing function of the frequency, the amplitude in this higher frequency range is much smaller, thus requiring higher accuracy in observations in order to estimate the amplitude reliably. We also find that for the higher frequency range ($3.5\le\nu\le5.5$ mHz) the fitted values of τ and γ are close to those predicted by the asymptotic theory (see Table 1), while at lower frequencies the fitted values are somewhat higher.

For the Sun it is possible to consider only intermediate-ℓ values to find the extent of overshoot, as has been done in the present work, since observations exist for many ℓ values. Observations of other stars are not, however, expected to give us any information about frequencies with $\ell>4$. We have therefore tried to see if it is possible to extract the oscillatory signal in the frequencies with $\ell\le4$ from our computed models. Only the fourth difference is considered, since that seems to give the best results. Fig. 12 shows our results using only the modes with $\ell\le4$, while Fig. 11(b) shows the $A-\tau$ diagram with the results for all models. It is clear that, even with the limited number of points, it is indeed possible to extract the oscillatory part and calculate its amplitude. Another advantage of the low-ℓ modes is that the ℓ dependence in both the oscillatory and the smooth component is not significant, and hence it is easier to obtain

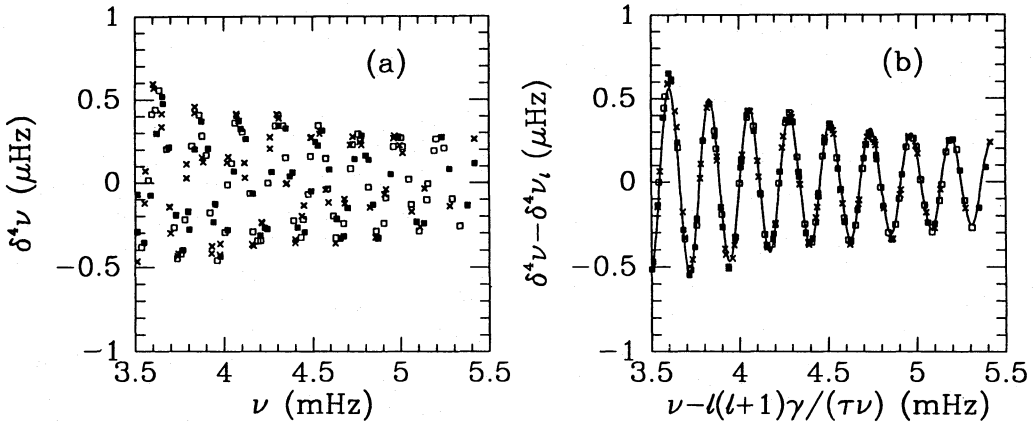

Figure 10. The fourth difference of frequencies computed for model M1 for $5 \le \ell \le 20$, and ν in the range 3.5–5.5 mHz. (a) shows the difference $\delta^4\nu$, while (b) shows the fit to the difference plotted after removing the ℓ dependence. The different symbols have the same meanings as in Fig. 4.

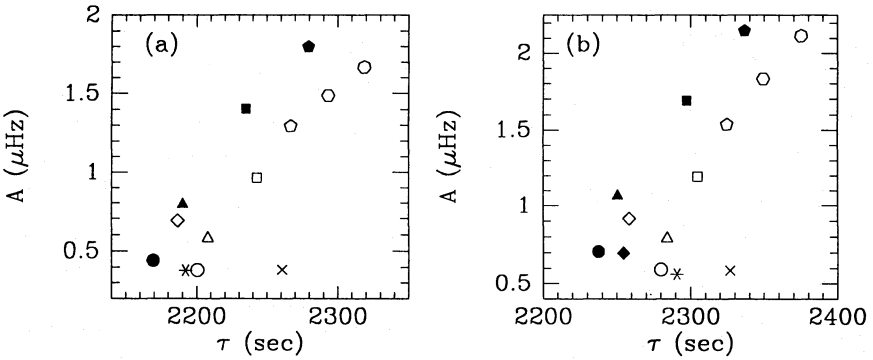

Figure 11. The amplitude A and the acoustic depth τ of the discontinuity for the different models for the fourth difference for (a) frequencies in the range 3.5–5.5 mHz for $5 \le \ell \le 20$ and (b) frequencies in the range 2.0–5.0 mHz for $0 \le \ell \le 4$. The different symbols have the same meanings as in Fig. 9. Points corresponding to models M7 and M11 overlap in (a) and hence the point for M11 cannot be seen distinctly.

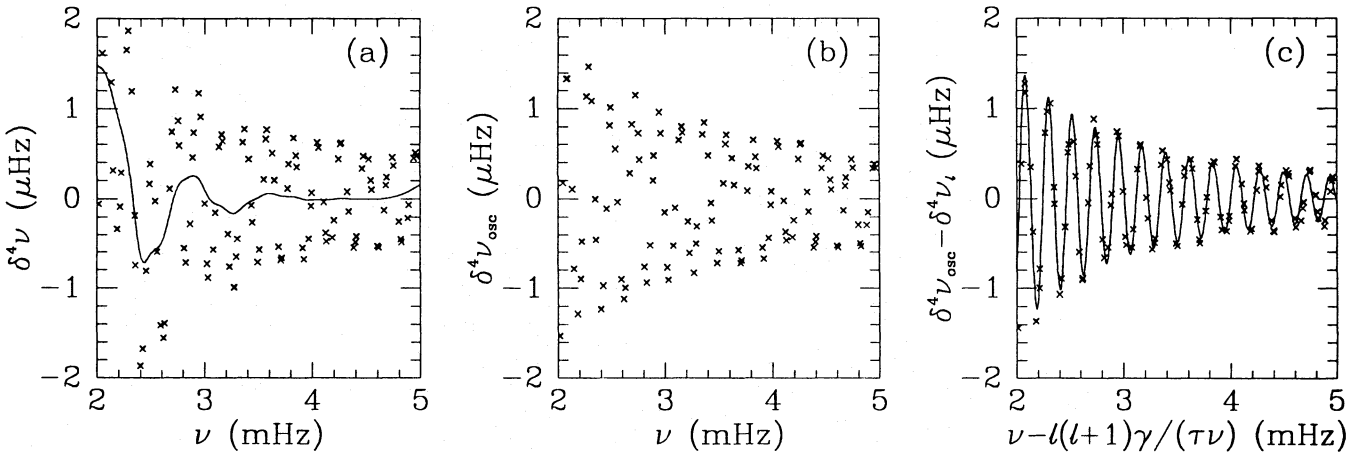

Figure 12. The fourth difference of the frequencies computed for model M1 for $0 \le \ell \le 4$, with ν in the range 2.0–5.0 mHz, is shown in (a). The curve defines the smooth part, which is removed to get the oscillatory part shown in (b). (c) shows the fit to the oscillatory part of the differences.

the fits. The observed frequencies for low-ℓ solar p-modes, however, have too large an error to be useful. The median of the variance in the fourth differences of the observed frequencies of Libbrecht et al. (1990) is 1.66 μHz for $0 \le \ell \le 4$ and the frequency range of 2–3.5 mHz. This is more than four times that for $5 \le \ell \le 20$ in the same frequency range. Thus the median of the errors is about twice the amplitude of the oscillatory part in the observed frequencies. Similarly, the

observed frequencies for low-ℓ modes from full disc measurements (e.g. Elsworth et al. 1991) also have comparable or larger errors. In fact, the low-ℓ frequencies in Libbrecht et al. (1990) have also been obtained from full disc observations and hence have larger errors as compared to intermediate-ℓ frequencies. Because of the large errors, it is not possible to extract the oscillatory part from the observed solar frequencies for low-ℓ modes.

4 CONCLUSIONS

In the present work we have attempted to infer the extent of overshoot below the solar convection zone using the amplitude of the oscillatory component in the frequency as a function of the radial order n. We have demonstrated that the present technique is able to distinguish between models with different extents of overshoot as well as with different depths of the convection zone (cf. Fig. 9). The amplitude mainly depends on the extent of overshoot, apart from the opacity gradient at the base of the convection zone, while τ essentially measures the depth of the adiabatic layer. The solar data appear to be consistent with model M1, which has no overshoot and is computed using the OPAL opacities. The depth of the convection zone in this model is the same as that inferred from helioseismic data by Christensen-Dalsgaard et al. (1991). Nevertheless, for a given extent of overshoot the amplitude does depend on the opacity gradient at the base of the convection zone, because the 'severity' of discontinuity in the temperature gradient is controlled by the opacity gradient. For example, models M1, M7, M11, M12 and M14 have no overshoot, but the amplitudes are not the same for all these models.

It may be noted that the results obtained for each of the differences are consistent with one another, thus indicating that the uncertainties in removing the smooth part and in the fitting process are not very significant. Further, the final A–τ diagram does not appear to depend crucially on the form of the function used for fitting, since Basu et al. (1993) obtained very similar results using a different form where the amplitude is independent of ℓ. Similarly, our results are consistent with those of Monteiro et al. (1993a,b), even though they used a very different form for fitting the frequency or the second derivative computed using splines.

Neglecting systematic errors due to uncertainties in the opacities and the presence of other force fields, we can put a 2σ upper limit of $0.1H_p$ on the extent of overshoot. On the other hand, if we assume that the Sun does have an overshoot layer of thickness $0.1H_p$, then, using the crude estimates given in Section 3 (cf. equation 20), it can be seen that the opacity gradient at the base of the solar convection zone will have to be reduced by a factor of ≈ 1.55 to get the quoted amplitude. A change of this magnitude in the opacity gradient does not appear to be likely. It may be noted that this change cannot arise because of differences in the depth of the convection zone, since that is known fairly accurately (Christensen-Dalsgaard et al. 1991) and, moreover, the value of τ will change with the depth of convection zone. Similarly, considering an intermediate scenario, if we add the 1σ error bar to the quoted amplitude for the observed frequencies, then the resulting amplitude will be consistent with an overshoot of $0.1H_p$ provided that the opacity gradient at the base of the solar convection zone is reduced by about 20 per cent. Of course, the presence of a few-megagauss magnetic field below the base of the convection zone may reduce the amplitude of the oscillatory component in the frequencies. The observed frequencies can be consistent with an overshoot of $0.1H_p$ provided there is a magnetic field of about 10^6 G below the base of the convection zone.

In principle, it is possible to apply this technique to estimate the extent of overshoot below the base of the outer convection zone in other stars also, using the frequencies of low-ℓ modes. For massive stars with convective cores there will be another discontinuity at the boundary of the convective core. This discontinuity should also contribute an oscillatory component to the frequencies. However, in our simple model in Section 2, we can measure the acoustic depth from either boundary. For the convective core the acoustic depth as measured from the centre is rather small, thus giving rise to an oscillatory signal with large wavelength, which may not be easily distinguishable from uncertain contributions from the surface layers. Thus it may not be possible to use this technique to measure the extent of overshoot above the stellar convective cores.

ACKNOWLEDGMENTS

We thank S. M. Chitre, J. Christensen-Dalsgaard and D. O. Gough for valuable discussions, and F. J. Rogers for sending us the opacity tables.

REFERENCES

Antia H. M., Chitre S. M., 1993, ApJ, 413, 778
Antia H. M., Chitre S. M., Narasimha D., 1984, ApJ, 282, 574
Bahcall J. N., Heubner W. F., Lubow S. H., Parker P. D., Ulrich R. K., 1982, Rev. Mod. Phys., 54, 767
Basu S., Antia H. M., Narasimha D., 1993, Bull. Astron. Soc. India, in press
Berthomieu G., Morel P., Provost J., Zahn J.-P., 1993, in Weiss W. W., Baglin A., eds, Proc. IAU Colloq. 137, ASP Conf. Ser. 40, Inside the Stars. Astron. Soc. Pac., San Francisco, p. 60
Christensen-Dalsgaard J., Berthomieu G., 1991, in Cox A. N., Livingston W. C., Matthews M., eds, Solar Interior and Atmosphere. Space Science Series, University of Arizona Press, Tucson, p. 401
Christensen-Dalsgaard J., Gough D. O., Thompson M. J., 1991, ApJ, 378, 413
Cox A. N., Tabor J. E., 1976, ApJS, 31, 271
Deardorff J. W., Willis G. E., Lilly D. K., 1969, J. Fluid Mech., 35, 7
Deubner F.-L., Gough D. O., 1984, ARA&A, 22, 593
Elsworth Y., Howe R., Isaak G. R., McLeod C. P., New R., 1991, MNRAS, 251, 7P
Gough D. O., 1990, in Osaki Y., Shibahashi H., eds, Lecture Notes in Physics 367. Springer, Berlin, p. 283
Gough D. O., Sekii T., 1993, in Brown T. M., ed., Proc. GONG 1992: Seismic Investigation of the Sun and Stars, ASP Conf. Ser. 42. Astron. Soc. Pac., San Francisco, p. 177
Hurlburt N. E., Toomre J., Massaguer J. M., 1986, ApJ, 311, 563
Keil S. L., Canfield R. C., 1978, A&A, 70, 169
Libbrecht K. G., Woodard M. F., Kaufman J. M., 1990, ApJS, 74, 1129
Monteiro M. J. P. F. G., Christensen-Dalsgaard J., Thompson M. J., 1993a, in Weiss W. W., Baglin A., eds, Proc. IAU Colloq. 137, ASP Conf. Ser. 40, Inside the Stars. Astron. Soc. Pac., San Francisco, p. 557
Monteiro M. J. P. F. G., Christensen-Dalsgaard J., Thompson M. J., 1993b, in Brown T. M., ed., Proc. GONG 1992: Seismic Investi-

gation of the Sun and Stars, ASP Conf. Ser. 42. Astron Soc. Pac., San Francisco, p. 253
Monteiro M. J. P. F. G., Christensen-Dalsgaard J., Thompson M. J., 1994, A&A, in press
Renzini A., 1987, A&A, 188, 49
Rogers F. J., Iglesias C. A., 1992, ApJS, 79, 507
Roxburgh I. W., Vorontsov S. V., 1993, in Brown T. M., ed., Proc. GONG 1992: Seismic Investigation of the Sun and Stars, ASP Conf. Ser. 42. Astron. Soc. Pac., San Francisco, p. 169
Stothers R. B., Chin C.-W., 1992, ApJ, 390, 136
Townsend A. A., 1966, Q. J. R. Meteorol. Soc., 90, 248
Zahn J.-P., 1991, A&A, 252, 1779